International Journal of Biological Macromolecules 273 (2024) 132971

Contents lists available at ScienceDirect

International Journal of Biological Macromolecules

journal homepage: www.elsevier.com/locate/ijbiomac

Maleic anhydride-functionalized cellulose nanocrystal-stabilized high internal phase Pickering emulsion for pesticide delivery

Chao Wu, Jun Li *, Jia-wei Ding, Hui Jiang, Hui-fen Su, De-qiang Li

College of Chemistry and Chemical Engineering, Xinjiang Agricultural University, Urumchi 830052, Xinjiang, PR China

ARTICLE INFO

Keywords:
Pesticide delivery
High internal phase Pickering emulsion
Cellulose

ABSTRACT

The salt-responsiveness of Pickering emulsions has significantly influenced their applications due to the large amount of salt on the surface of plant leaves. The present study provided a maleic anhydride-functionalized cellulose nanocrystal-stabilized high internal phase Pickering emulsion (MACNCs-HIPPEs) that was stable to high-concentration salt and used for pesticide delivery. The stability of MACNCs-HIPPEs was investigated by adjusting the oil-phase volume fraction (φ), the MACNCs concentration, NaCl dosages, and the rheological properties. The high internal phase Pickering emulsion was obtained at φ of 0.8 and MACNCs concentration of 2wt% and showed excellent salt stability (NaCl, 1200 mM) and significant storage stability (60 days). The sustained release of imidacloprid (IMI) from imidacloprid-loaded MACNCs-HIPPEs (IMI@MACNCs-HIPPEs) showed a positive correlation to the temperature (15°C, 25°C, 35°C), indicating clear thermo-responsiveness of the prepared pesticide formulation. The test of spread and retention of IMI@MACNCs-HIPPEs on the leaf surface showed a significant advantage compared with the commercial IMI water dispersible granules (CG). All the advantages mentioned above showed the excellent potential of the MACNCs-HIPPEs in delivering lipophilic pesticides.

1. Introduction

Pesticides accompany almost every stage of crop growth and resist the erosion of pests and bacteria for their normal growth, which also directly ensures the excellent yield of crops and makes an invaluable contribution to human food security [1]. However, poor efficiency has been the crux in pesticide applications, i.e., less than 1% of the critical ingredients to be applied to crops, which significantly increases the overuse of pesticides and poses particular risks to human health and the soil environment [2,3]. Various micron and nano-scale carriers, including emulsions, capsules, and gels, have been consequently developed for pesticide delivery that can effectively improve the utilization rate of pesticides, reduce their dosage, prolong their duration, and improve their adverse effects [4]. The currently complex preparation techniques and non-degradable feedstocks determine the environmental unfriendliness and high cost of the as-prepared pesticide delivery carriers, which thus need to be improved [5].

Compared with the conventional emulsion, Pickering emulsion routes have been developed into an excellent pesticide encapsulation technique due to the irreversible adsorption of stabilizer on the oil-water interface that endowed Pickering emulsion-based pesticide carrier with great stabilization. Moreover, the small size and large surface area ensure Pickering emulsion droplets can be uniformly attached to leaves, thus improving the utilization rate of pesticides [6] and consequently reducing the toxicity of pesticides to non-target organisms and protecting local ecological diversity [7,8]. Inorganic nanoparticles (e.g., SiO_2, TiO_2, and ZnO) have been successfully used to stabilize Pickering emulsions for pesticide delivery but cannot be degraded in the natural environment. The large-scale usage undoubtedly increases the resistance to the development of pesticide delivery because of the consequent immune system disorders [9], organ damage [10,11], and metabolic disorders [12,13]. The biodegradability and compatibility of macromolecules make them rapidly applied to Pickering emulsion, among which cellulose is deeply concerned. Cellulose nanocrystals (CNCs) are representative of the cellulose derivative and have been widely used. However, the generated sulfate hemi-ester groups and the remaining hydroxyl groups on their surface caused strong hydrophilicity, which is a complex problem in emulsion stabilization. The large number of active hydroxyl groups on the surface also supports surface modification, thus preparing Pickering emulsion with more feasibility and rich properties.

* Corresponding author.
E-mail addresses: junli107@163.com (J. Li), lsx20131120a@163.com, ldq@xjau.edu.cn (D.-q. Li).

https://doi.org/10.1016/j.ijbiomac.2024.132971
Received 19 December 2023; Received in revised form 24 May 2024; Accepted 5 June 2024
Available online 14 June 2024

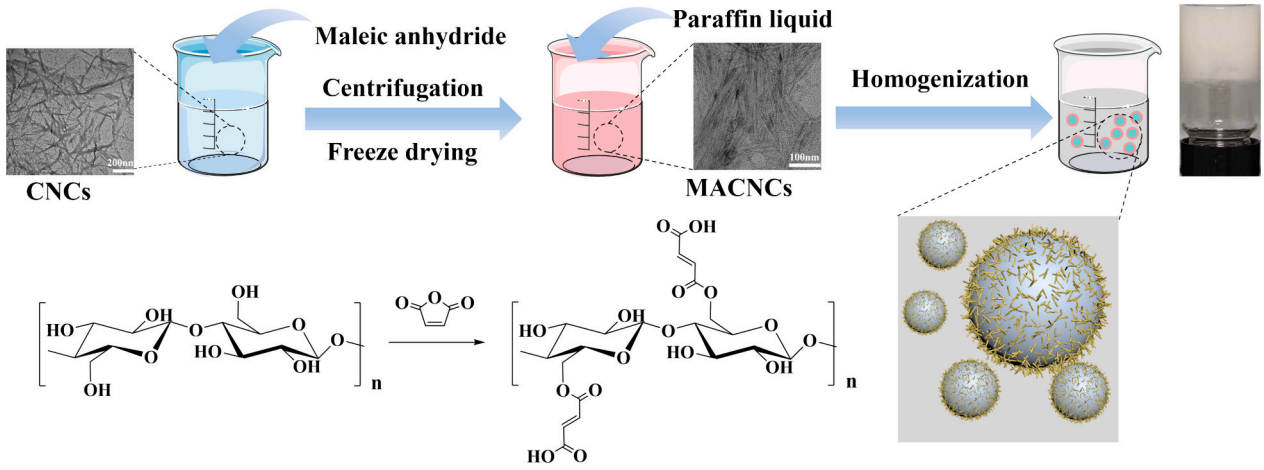

Fig. 1. Schematic of preparation of MACNCs and MACNCs-HIPPEs.

High internal phase Pickering emulsions (HIPPEs) are a special kind of Pickering emulsion, which has all the advantages of Pickering emulsion while maintaining a high elasticity and high viscosity [14]. It also has the following benefits in pesticide delivery: (1) higher stability than Pickering emulsion that overcomes instability phenomena such as droplet agglomeration and Ostwald curing [15,16]. (2) more green than traditional emulsions that avoid using aromatic toxic reagents (e.g., toluene) [17]. (3) higher loading capacity due to the high internal phase volume fraction of greater than 74%; (4) strong protection capability from photodegradation for pesticides [18]. Thus, HIPPEs have been used to deliver active ingredients in various areas such as functional food and drug delivery. Moreover, there is still a blank for CNCs-based HIPPEs in pesticide delivery.

The objective of the present study was to adjust the wetting of CNCs and further study the feasibility of forming HIPPEs for pesticide delivery. The CNCs were modified with maleic anhydride (MA) and characterized by FTIR, XRD, and contact angle techniques. Also, the ζ-Potential and z-average diameter of maleic anhydride-functionalized CNCs (MACNCs) in dispersions with different NaCl concentrations were determined. The MACNCs stabilized high internal phase Pickering emulsions (MACNCs-HIPPEs) were prepared for pesticide delivery, and their stability was discussed by adjusting the oil-water ratios and salt concentrations. In addition, the rheology and imidacloprid release of the MACNCs-HIPPEs were performed. The results show that the modified cellulose can be used as a single stabilizer for forming HIPPEs, and the sustained release of IMI can reach 48 h, which is of research value for pesticide delivery. Moreover, these HIPPEs can be used to deliver other oleophilic pesticides such as phoxim and dimethoate.

2. Materials and methods

2.1. Materials

Cotton was supplied by Xinjiang Production and construction Corps eighth Agricultural Division. Sulfuric acid with 98% purity was provided by Xilong Scientific Co., Ltd. (Guangdong, China). *N*,*N*-dimethylformamide (DMF) with 99.5% purity was purchased from Tianjin Yongsheng Fine Chemical Co., Ltd. (Tianjin, China). Maleic anhydride (MA) with 99.5% purity was obtained from Shanghai Jingxi Chemical Technology Co., Ltd. (Shanghai, China). Ethanol absolute with 99.7% purity was supplied by Tianjin Zhiyuan Chemical Reagent Co., Ltd. (Tianjin, China). Paraffin liquid used as model oil was provided by Shanghai Rhawn Chemical Technology Co., Ltd. (Shanghai, China). Sodium chloride with 99.5% purity was purchased from Tianjin Zhiyuan Chemical Reagent Co., Ltd. (Tianjin, China). Methanol with 99.5% purity was obtained from Tianjin Xinbo Special Chemical Co., Ltd. (Tianjin, China). Imidacloprid (IMI) with 95% purity was provided by Shanghai Yuanye Bio-Technology Co., Ltd. (Shanghai, China).

2.2. Preparation of CNCs

Cotton was cut to less than 1 cm and directly used to prepare CNCs via the sulfuric acid hydrolysis method with a few modifications [19]. Twenty grams of cotton were added into 200 g of sulfuric acid solution with a concentration of 64wt% with mechanical agitation (300 rpm) at 50°C for 1.5 h. Then, 2000 mL of deionized water was added to terminate the hydrolyzation reaction. The diluent was stood till a distinct stratification occurred, and the lower dispersion was centrifuged to neutrality and freeze-dried to obtain solid CNCs.

2.3. Preparation of MACNCs

The modification of CNCs was applied based on previous methods with minor modifications (Fig. 1) [20]. Solid CNCs (3 g) were evenly dispersed in 60 mL DMF and stirred at 300 rpm for 0.5 h continuously, followed by adding 30 g of MA and stirring for another 0.5 h. The reaction temperature was raised to 120°C and carried out for 20 h. Then, 400 mL absolute ethanol was added and stirred continuously for 2 h to terminate the reaction. The reaction system was centrifuged at 7500 rpm for 10 min, and the lower precipitate was collected. The precipitate was washed with absolute ethanol three times to remove the MA and DMF completely. Finally, the precipitate was dispersed in deionized water and freeze-dried to obtain MACNCs.

2.4. Characterization of MACNCs

The MACNCs suspend carboxyl groups that originated from the MA, and thus, the content of the carboxyl group was the grafting amount of MA. The carboxyl group content of MACNCs was determined by conductometric titration [21]. MACNCs (0.3 g) were added to 100 mL of deionized water, and the pH value of the solution was adjusted to near 3 with 0.1 mol·L^{-1} HCl. It was evenly stirred with a magnetic stirrer and titrated with 0.05 mol·L^{-1} NaOH solution. Then, the conductivity of the solution was changed with the addition of NaOH solution till the pH reached around 11 (i.e., titration endpoint), which was measured on a conductivity meter (DDSJ-307F, China). According to the experimental data, the conductivity curves of the solution versus the volume of NaOH solution consumed were drawn, and the content of carboxyl groups was calculated using the following formula.

$$\text{Content of carboxyl groups}\left(\frac{\text{mmol}}{\text{g}}\right) = \frac{C_{NaOH}(V_1 - V_2)}{m} \quad (1)$$

where C_{NaOH} is the concentration of the titrated NaOH solution, V_1 is the volume of NaOH solution required to consume HCl in solution, V_2 is the volume of NaOH solution that consumes all acidic substances in the solution, m is the dry weight of the MACNCs sample.

The lyophilized CNCs and MACNCs were ground, mixed with KBr, and further laminated. The chemical variations of CNCs before and after the modification with MA were detected on a Nicolet iN10 MX FT-IR spectroscopy (Thermo Scientific, USA) in a scanning region of 4000-500 cm^{-1} at a resolution of 4 cm^{-1}. The X-ray diffraction patterns of CNCs and MACNCs were obtained on a Bruker D8 Advance diffractometer (Bruker, German) with Cu Kα radiation ranging from 5 to 80° at a rate of 2 °/min and operated at a power of 40 kV with a current of 40 mA. The crystallinity was calculated by Segal's method [22]:

$$CI = \left(\frac{I_{200} - I_{AM}}{I_{200}}\right) \quad (2)$$

where I_{200} is the peak intensity at the plane (200) in the XRD profile, and I_{AM} is the minimum intensity at the valley between the planes (200) and (110).

The ζ-potential and the size distribution profile of MACNCs suspensions (0.1%, *w/v*) at different NaCl concentrations were measured by the Malvern Zetasizer nanoseries (Nano-ZS90, UK). The thermo-stability of CNCs and MACNCs were tested on a thermogravimetric analyzer (Netzsch TG 209 F3 Tarsus, Germany) under nitrogen atmosphere at a heating rate of 10°C/min from 30°C to 800°C. Contact angle is a crucial parameter in judging the wettability of a substance. SL200KB contact angle goniometer (Solon Tech. Co., Ltd., Shanghai, China) was used to measure the three-phase contact angles of CNCs and MACNCs. The sample was pressed into tablets with 13 mm in diameter and 2 mm in thickness. Then, 3 μL of ultra-pure water was dropped on the surface, and the droplet behavior was captured by a video camera. The contact angles were calculated by fitting the droplet contour with the Laplace-Young equation.

2.5. Preparation of MACNCs-HIPPEs

MACNCs were pretreated by ultrasound under an ice bath. The facile route of MACNCs-HIPPEs preparation is shown in Fig. 1. All the emulsions were stabilized by MACNCs on a homogenizer (FSH-2A, China) at 12000 rpm for 3 min. The influences of NaCl concentration (μ, 0-1200 mM), proportions of paraffin liquid to MACNCs suspensions (φ, 0.1-0.9), and MACNCs suspension concentrations (0.5-4.0wt%) on the 24-hour stability of the MACNCs-HIPPEs were studied. Traditional droplet experiments were employed to judge the emulsion type. If the emulsion can be dispersed in water and not in liquid paraffin, the HIPPEs were an oil-in-water (O/W) type emulsion; otherwise, they were water-in-oil (W/O) type.

2.6. Characterization of HIPPEs

The HIPPEs were diluted with the same volume of water each time, and microstructures were observed on an MX-117P polarizing optical microscope (Shenzhen, China) with a camera (HK117PM, Shenzhen, China). The MCR 302 rheometer (Anton Paar) was used to test the rheological properties of HIPPEs at 25°C. The linear viscoelastic region of HIPPEs was tested in the strain range of 0.01-1000%, and the yield strain was measured by amplitude scanning mode. Then, a 0.2% strain was determined in the above-mentioned shear strain scanning. The HIPPEs were tested at different frequencies ranging from 0.01 to 100 Hz to record the elastic modulus (G") and loss modulus (G').

2.7. IMI loading and sustained release

According to the above-mentioned experimental result, the MACNCs-HIPPEs that were prepared at 2wt% of water phase concentration (i.e., the concentration of MACNCs) and the oil-water ratio of 8:2 without adding NaCl presented the best stability. Thus, these MACNCs-HIPPEs were employed to in situ load IMI to obtain IMI-loaded HIPPEs (IMI@MACNCs-HIPPEs). In detail, 10 mg of IMI was dissolved in 8 mL of liquid paraffin, followed by adding 2 mL of MACNCs solution to form a dispersion system, which was further homogenized at 12000 rpm for 3 min.

For the sustained release of IMI from the IMI@MACNCs-HIPPEs, 1 g of the IMI@MACNCs-HIPPEs was weighed and injected into a dialysis bag with an MWCO of 3500 Da that was put into 100 mL methanol-water (v/v=4:6) solution at different temperature (15°C, 25°C, and 35°C) under oscillation (200 rpm). Then, 3 mL of the sustained release media was sucked out at the preset time interval, and 3 mL of the initiating methanol solution was supplemented in time. The sucked emulsions were centrifugated at 10000 rpm for 5 min and filtrated by a millipore filter (0.22 μm), which were further scanned on a UV-Vis spectrophotometer to calculate the concentration of IMI in the sucked release media. The cumulative release amount of IMI was calculated using the following formula:

$$\text{Cumulative release rate} = \sum_{t=0}^{t} \frac{M_t}{M_0} \times 100\% \quad (3)$$

where M_t is the IMI released from microcapsules at the preset time interval, and M_0 is the total mass of IMI in IMI@MACNCs-HIPPEs.

2.8. Kinetics study of the release process

The release kinetics of IMI from IMI@MACNCs-HIPPEs was analyzed using zero-order, first-order, Higuchi, and Ritger Peppas models as follows [23].

$$\text{Zero} - \text{order model}: \frac{M_t}{M_\infty} = k_1 t \quad (4)$$

$$\text{First} - \text{order model}: \frac{M_t}{M_\infty} = 1 - exp^{-k_2 t} \quad (5)$$

$$\text{Higuchi model}: \frac{M_t}{M_\infty} = k_3 t^{\frac{1}{2}} \quad (6)$$

$$\text{Ritger Peppas model}: \frac{M_t}{M_\infty} = k_4 t^n \quad (7)$$

where M_t was the amount of drug released at time t, M_∞ was the maximal amount of the released drug at infinite time, k_i is the rate constant of pesticide, and n stood the diffusion exponent of Fickian diffusion ($n \leq 0.43$), non-Fickian ($0.43 < n < 0.85$), swelling control process ($n \geq 0.85$).

2.9. Spread and retention of IMI@MACNCs-HIPPEs on the leaf surface

The static contact angle of the emulsion on the leaf surface is an effective method to judge spreadability [24]. Cotton leaves were cut into strips and glued to the glass slide. IMI@MACNCs-HIPPEs at a concentration of 0.18 g/g to 0.2 g/g was sucked into a microsyringe and sprinkled on the leaf surface for measurement and recording with a contact angle instrument. All other operations were the same as the determination of the contact angle of MACNCs.

The retention of IMI@MACNCs-HIPPEs on cotton leaves was measured by the dipping method [25]. IMI@MACNCs-HIPPEs at a concentration of 0.18 g/g to 0.2 g/g was placed in the beaker, the tweezers and the beaker were weighed as W_1, the cotton leaves were divided into rectangles with an area of S, and the leaves were picked up with tweezers and immersed in the beaker for 10 s, and then left right above the beaker for 2 min. The weight of the beaker and the tweezers was weighed as W_2. The retention amount (R, mg/cm^2) of

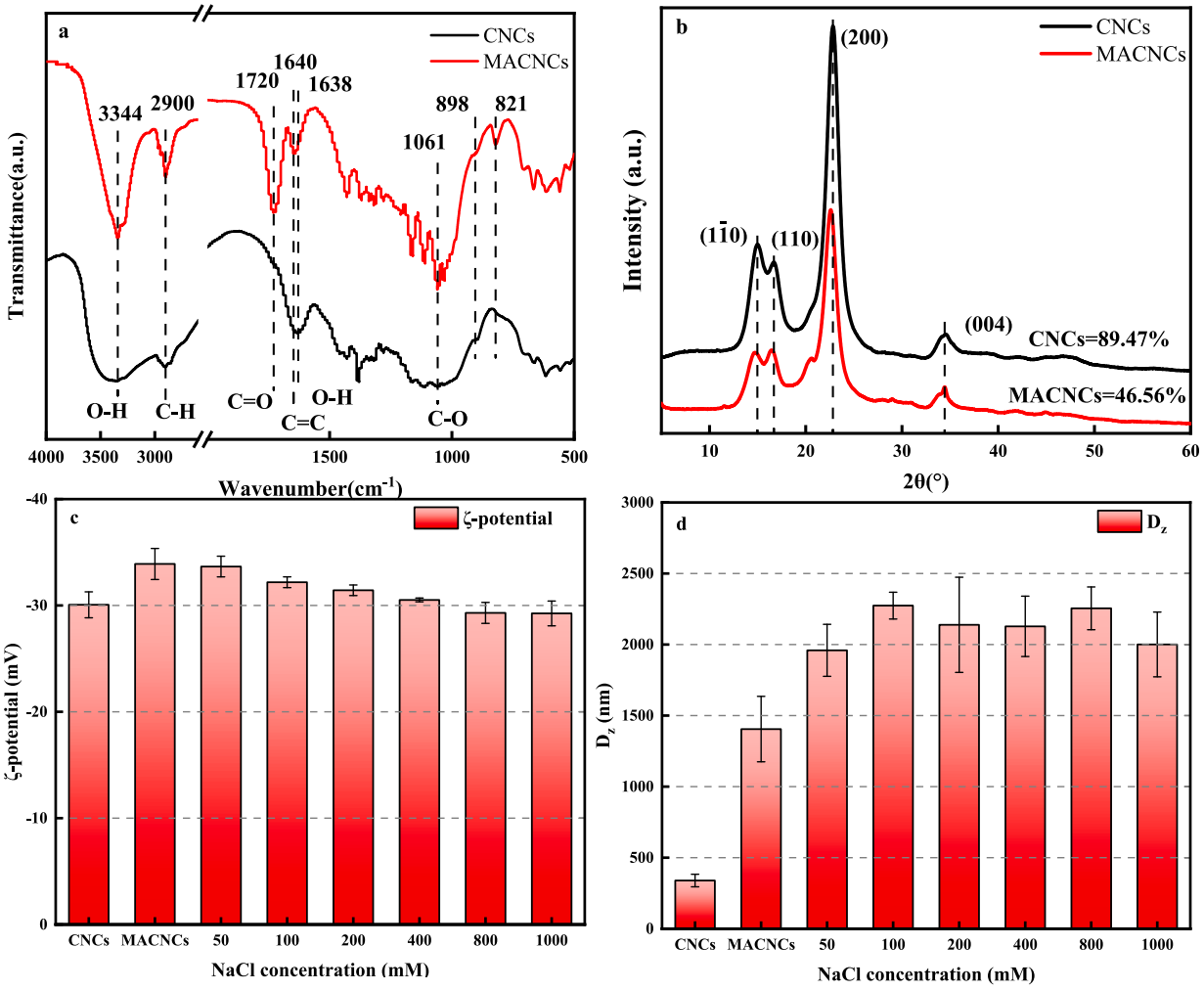

Fig. 2. Physicochemical characteristics of CNCs and MACNCs. (a) FT-IR spectra; (b) XRD patterns; (c and d) ζ-Potential and z-average diameter of CNCs and MACNCs with different NaCl concentrations.

IMI@MACNCs-HIPPEs on the surface of cotton leaves was calculated by $\boldsymbol{R} = (\boldsymbol{W_1} - \boldsymbol{W_2}) \times \boldsymbol{1000}/\boldsymbol{S}$.

Moreover, the IMI@MACNCs-HIPPEs and water were sprinkled on the surface of the cotton leaf with a dip angle of 60° from a syringe with a 0.7 mm needle, during which the retentions were also videoed.

3. Results and discussion

3.1. Physicochemical characteristics of CNCs and MACNCs

Solid nanoparticles can irreversibly adsorb on the oil-water interface to form a Pickering emulsion, during which they are partially wetted by the continuous phase and dispersed phase. The irreversible adsorption of solid particles at the oil-water interface is explained. The stable adsorption of solid particles at the interface is also a condition for the stability of high internal phase Pickering emulsion. It can be described by the formula: $\boldsymbol{\Delta G} = \boldsymbol{\pi R^2 \gamma_{ow}(1 \pm \cos\theta)^2}$, where R is the radius of solid particles, γ_{ow} is the surface tension of the oil-water interface, and θ is the three-phase contact angle of particles. The adsorption energy determines the difficulty of solid particles adsorbing at the oil-water interface. When θ approaches 90°, the solid particles have difficulty escaping from the oil-water interface due to the largest required desorption energy. In other words, the closer the contact angle is to 90°, the higher the stability of the emulsion [26]. The wide existence of sulfate hemi-ester and hydroxyl groups determined the strong hydrophilicity of CNCs and the consequent instability of native CNCs-stabilized Pickering emulsions [27]. Thus, we modified CNCs with MA to decrease their hydrophilia. After the modification, the contact angles increased from 52.7° to 73.0° (Fig. S3), CNCs are highly hydrophilic due to the abundant sulfate hemi-ester groups and hydroxyl groups on the surface. The modification with maleic anhydride introduced a carboxyl group and seemed to increase the hydrophilia of the resultant CNCs (i.e., MACNCs). However, this process also enhanced the content of hydrophobic groups (i.e., ester and vinyl groups), which was twice the amount of hydrophilic groups (i.e., carboxyl group) [28,29]. Thus, the hydrophilicity is reduced. This also indicates that the MACNCs could form stable O/W Pickering emulsions.

The FT-IR technique was employed to characterize the chemical variation of CNCs before and after the functionalization by MA (i.e., CNCs and MACNCs), and the results are shown in Fig. 2a. CNCs and MACNCs share the same absorption peaks at 3400 cm^{-1}, 2900 cm^{-1}, 1061 cm^{-1}, and 898 cm^{-1} that were ascribed to the -OH stretching vibration, C-H stretching vibration, C-O stretching vibration and β-glucosidic bonds of the cellulose molecules [30]. It can be noticed that the structure of MACNCs has changed to some extent, and new bands can be observed in the MACNCs spectrum. The strong and sharp absorption peak located at 1720 cm^{-1} was the stretching vibration of C=O in the free carboxyl groups, indicating the formation of ester bonds. The new peak at 821 cm^{-1} may be the out-of-plane deformation of the carboxyl group on MA [31]. The different peak at 3334 cm^{-1} was found in the MACNCs spectrum, belonging to the intermolecular hydrogen

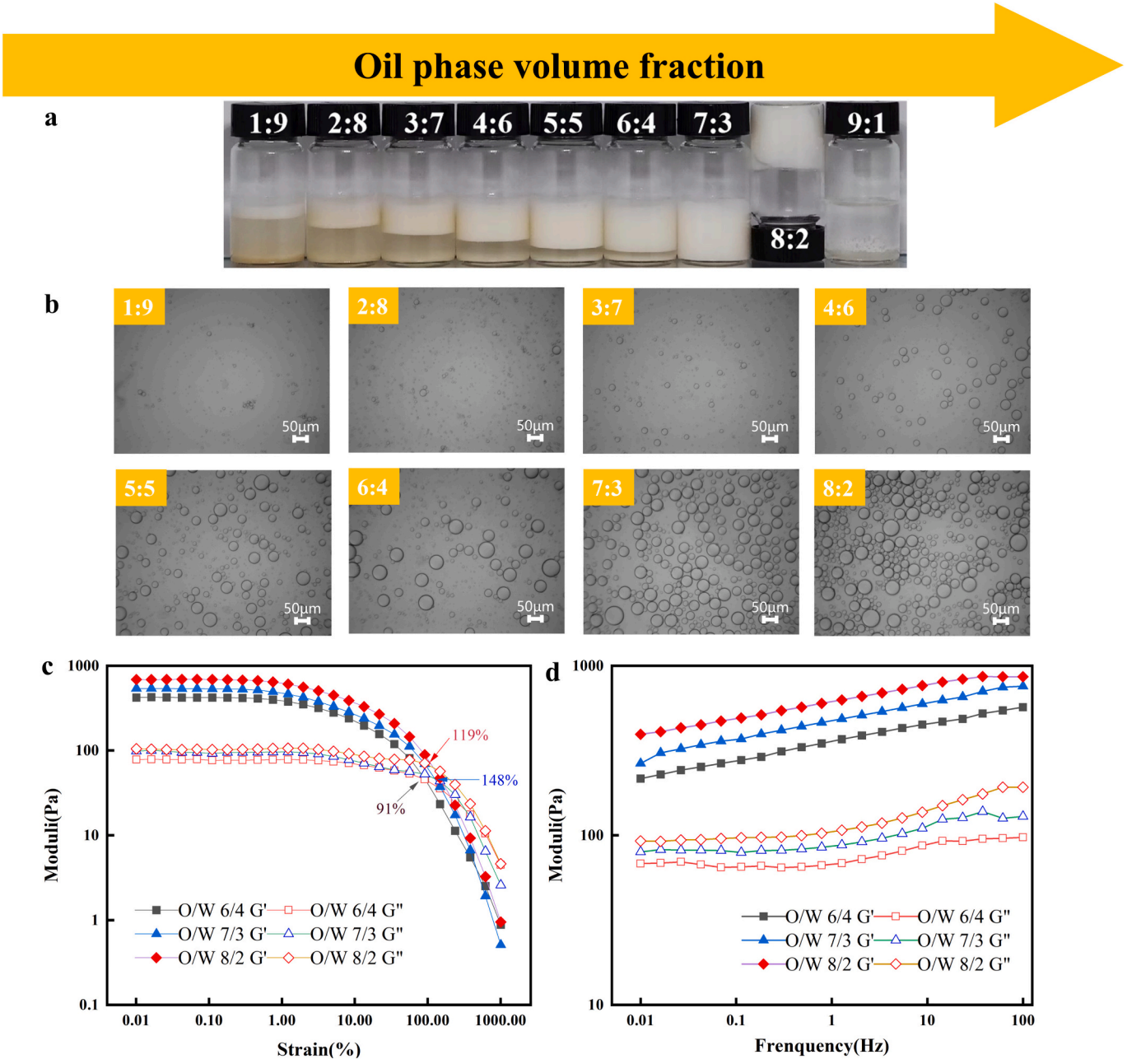

Fig. 3. MACNCs-stabilized Pickering emulsion with aqueous phase concentration of 2wt% and φ range of 0.1-0.9: (a) Digital photos; (b) optical microscopy images; (c) strain sweep test of the MACNCs-stabilized Pickering emulsion with O/W ratios of 6:4, 7:3, and 8:2; and (d) frequency sweep test of the as-prepared MACNCs-stabilized Pickering emulsion with O/W ratios of 6:4, 7:3, and 8:2.

bond in the crystalline region of cellulose [32]. In addition, the absorption peak at 1640 cm^{-1} is shifted, which may be caused by the overlap of the absorption peak of water in CNCs and the deformation vibration peak of the C=C linkage [33]. In the suspended accessory, the amount of alkenyl equaled that of carboxyl groups. The content of the carboxyl group was calculated as 0.27 mmol/g via the conductance titration (Fig. S1). Moreover, the three hydroxyl groups, linked to the C atoms at the C2, C3, and C6 of glucose, showed different reactivity. In detail, C6 primary alcohol is ten times more active than C2 and C3 secondary alcohols due to the free rotation of C5 and C6 bonds [34]. Therefore, the OH of C6 of CNCs preferentially reacts with MA.

The XRD patterns could reflect the crystallization behavior of CNCs and their derivatives. Fig. 2b shows that the MACNCs had the characteristic peaks of cellulose appearing on the 101 and 002 crystal planes, indicating their crystalline form of cellulose I. The only difference was that the intensity of the characteristic peaks decreased, and the crystallinity of CNCs and MACNCs was 89.47% and 46.56%, respectively. This phenomenon may be due to surface grafting or coating, and a similar trend can be found in the polyacrylamide-modified CNCs [35]. Also, the diffraction peaks did not shift, indicating that the modification did not break the native crystal structure. This result proved that the functionalization only occurred on the surface hydroxyl groups on of CNCs [36]. The surface-pendent carboxyl groups were weakly dissociated functional groups. They undoubtedly induced a shielding of sulfate hemi-ester groups that would endow the MACNCs with sluggishness to the ionic strength, viz., the MACNCs-stabilized Pickering emulsions may exhibit the stability to the salt ions. In addition, the micromorphology of CNCs and MACNCs is basically the same (Fig. S2).

As discussed above, the modification significantly influenced the accessibility of the surface charge. Thus, we determined the ζ-Potential

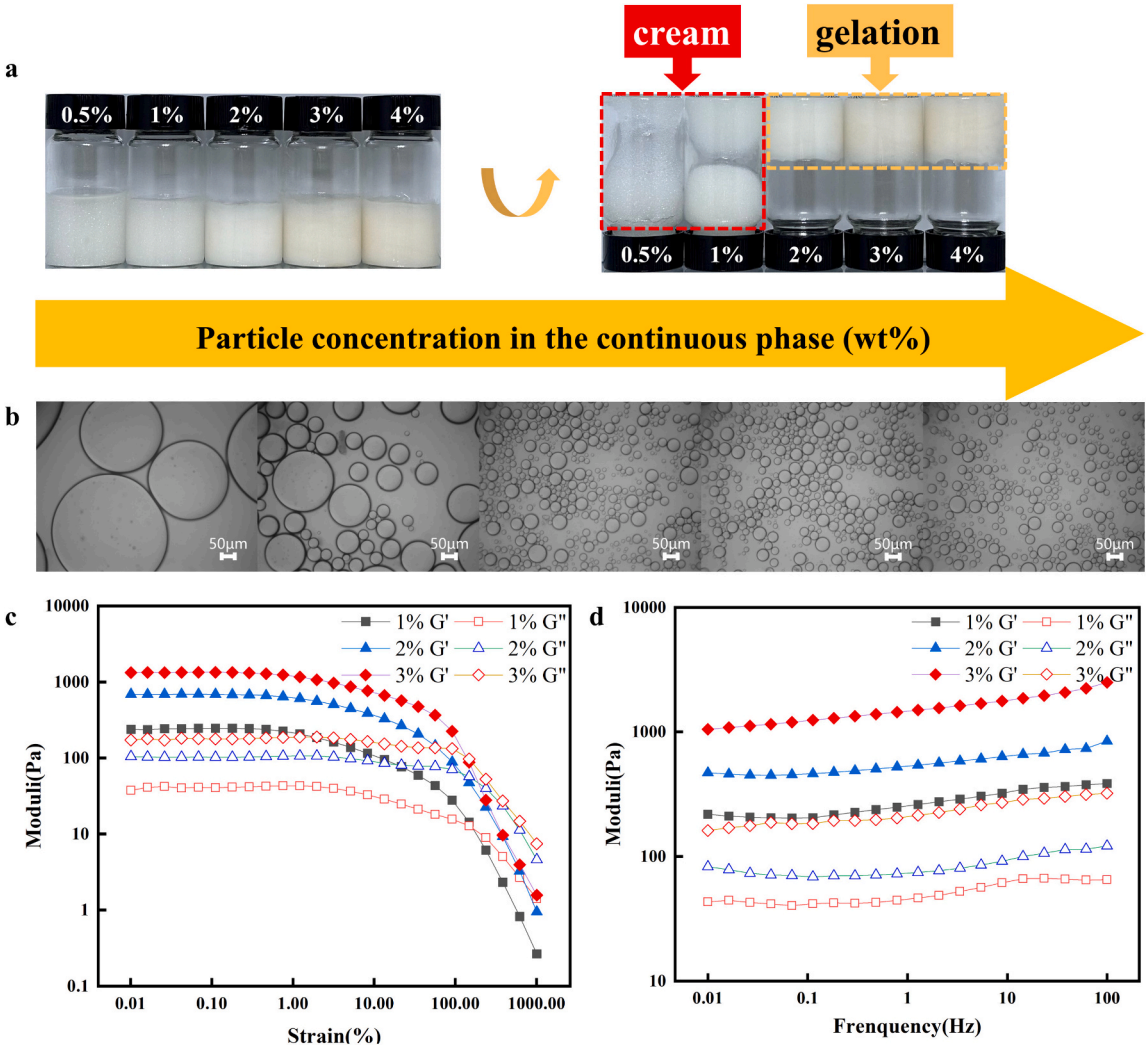

Fig. 4. MACNCs-HIPPEs with MACNCs concentration of 0.5-4wt% and φ value of 0.8: (a) digital photos; (b) optical microscopy images with MACNCs concentrations of 0.5, 1, 2, 3, and 4wt% (from left to right); (c) strain sweep test of the MACNCs-HIPPEs; and (d) frequency sweep test of the as-prepared MACNCs-HIPPEs at strain of 0.2%.

and z-average diameter (D_z) of CNCs and MACNCs, and the results are shown in Fig. 2c and d. In the pure solutions, the CNCs and MACNCs showed the difference in the ζ-Potential (-30.05 mV and -33.91 mV), which were induced by surface-suspended carboxyl groups [37]. When different dosages of NaCl were added to the solution, the ζ-Potential of MACNCs presented a decreased trend, but that was slight. In detail, the ζ-Potential of MACNCs shifted from -33.91 mV to -29.3 mV when the NaCl concentration increased to 1000 mmol/L (i.e., 58.5 mg/mL). This result was much different from our previous study, in which the ζ-Potential of CNCs changed from -42.6 mV to -17.8 mV with the NaCl concentration increased to 20 mg/mL [38]. The difference manifested the pivotal role of maleyl groups that can form a barrier around the CNCs, consequently shielding the NaCl. This situation was also found in octenyl succinic anhydride-functionalized CNCs [39]. Thus, the surface functionalization of MA significantly influenced the surface chemistry of CNCs.

The modification of maleic anhydride increased the hydrophobicity of CNCs and caused agglomeration, resulting in a larger particle size, which caused the PDI value to increase from 0.4915 to 0.8889. For solid particles, the shielding of surface charges undoubtedly induced the agglomeration. Thus, we also obtained the changes in the D_z of CNCs and MACNCs by adding different dosages of NaCl (Fig. 2d). The D_z of MACNCs was much higher than that of CNCs, which is opposite to the result of ζ-Potential, indicating that the increased surface charge density did not prevent the agglomeration of the nanoparticles. When the NaCl was added to the solution, the MACNCs showed changes in the D_z but did not increase, and the PDI value also was not significantly changed (Table S1). In this process, the maleyl groups might form a buffer area that prevents agglomeration [40,41].

The thermal stability of CNCs and MACNCs was investigated by the TG-DTG technique. The weight loss below 200°C can be ascribed to the evaporation of free and adsorbed water that can form strong hydration with sulfate hemi-ester and hydroxyl groups [42]. For the thermostability of CNCs, the decomposition temperature appeared at a peak value of 291°C, and a mass loss of about 76% was obtained when the temperature increased to 336°C. Different from CNCs, MA-functionalized CNCs showed a carried-forward decomposition peak temperature of 314°C, indicating that the surface coating inhibited the catalytic degradation by sulfate hemiester groups [35]. The decrease in thermal stability of MACNCs may be due to the breakdown of intermolecular hydrogen bonds and weak intermolecular interaction caused by modification reaction [43].

3.2. *Influence of O/W ratios on the formation of MACNCs-HIPPEs*

The macro visual and microscope images of MACNCs-stabilized

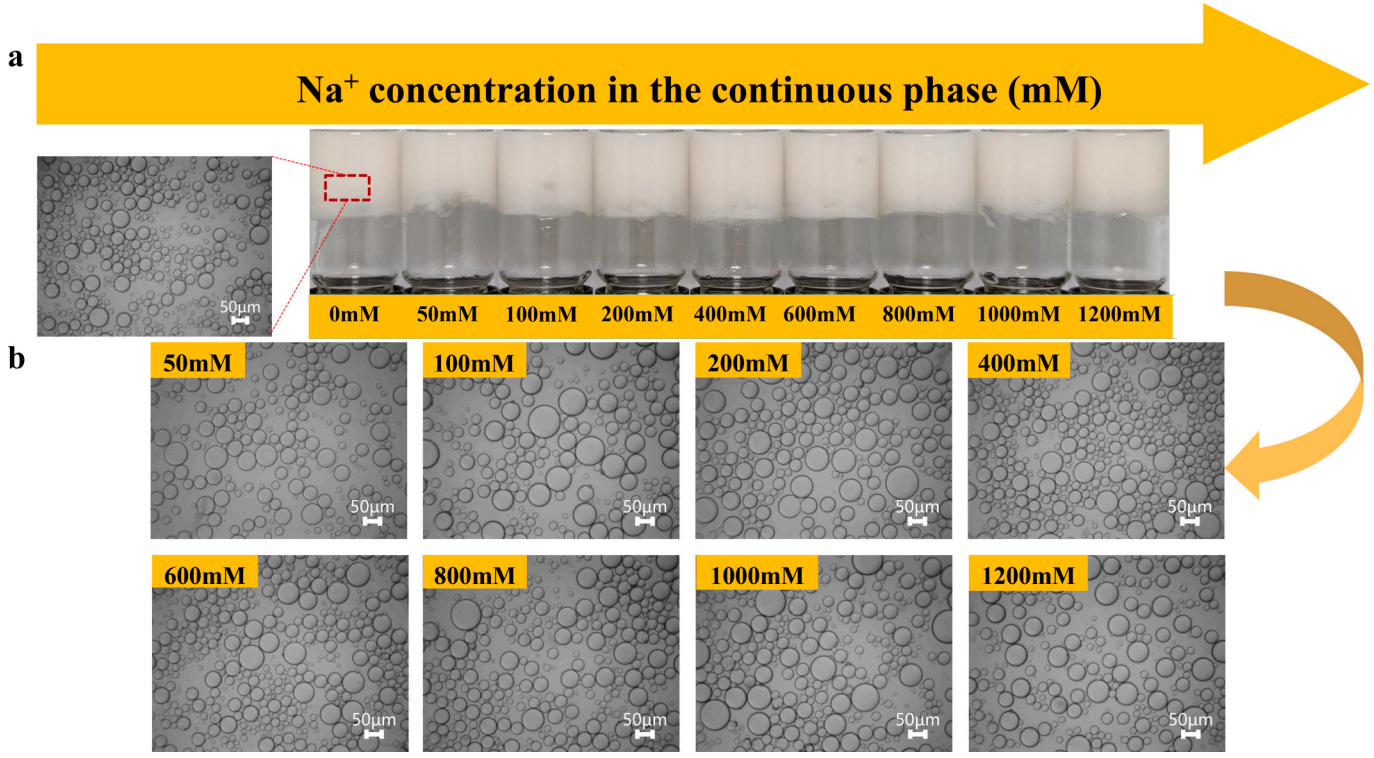

Fig. 5. The stability of as-prepared MACNCs-HIPPEs (MACNCs concentration of 2wt%, and φ of 0.8) to NaCl (0-1200 mM): (a) digital photos; (b) optical microscopy images.

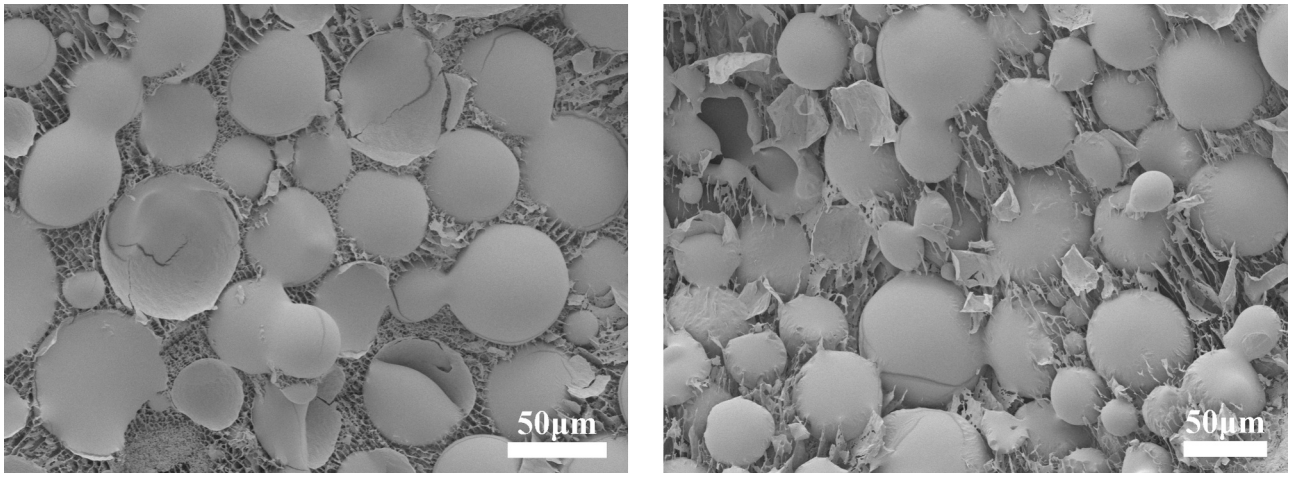

Fig. 6. Cyro-SEM images of MACNCs-HIPPEs (MACNCs concentration of 2wt%, and φ of 0.8) to NaCl (0 mM).

Pickering emulsion obtained at different φ (0.1-0.9) are shown in Fig. 3a and Fig. 3b, respectively. The emulsion volumes were enhanced with the increasing φ followed by forming HIPPEs (Fig. 3a). The optical microscopy images manifested that the emulsion droplets increased with the increasing φ (Fig. 3b and Fig. S5). This phenomenon was because of the fixed maximum interface area occupied by particles in each water phase, and the increased droplet size could keep the unchanged interface area [44]. It can be seen that MACNCs-HIPPEs presented two layers (i.e., upper cream and underlying water phase) when the φ was less than 0.7. When φ achieved 0.8, the emulsion droplets were particularly dense, showing extreme accumulation, as well as a non-mobile state in macroscopic, which was a feature of HIPPEs [45]. Moreover, this emulsion remained in the same state, even if it was stored for one month. Oil-water separation appeared when the φ increased to 0.9 due to the droplet coalescence and Ostwald ripening [46,47].

The test of rheological properties was performed to prove the gel-like characteristics of HIPPEs. The results are shown in Fig. 3c. The storage modulus (G') was much higher than the loss modulus (G") of the as-prepared MACNCs-stabilized Pickering emulsion at different φ in the low strain range, which indicated the elastic behavior and solid-like properties at this time [48]. The curves of G' intersected the curves of G" as the increase in strain, manifesting the collapse of the network and a gel-sol transition [49]. Moreover, the G' of the MACNCs-HIPPEs increased with improvement in φ; these results were consistent with the results shown in the optical microscopy images, viz., enhanced φ contributed to form the gel network structure of HIPPEs [50]. Fig. 3d showed the frequency dependence test of MACNCs-HIPPEs at different φ. All the G' were higher than G", showing the dominant role of the

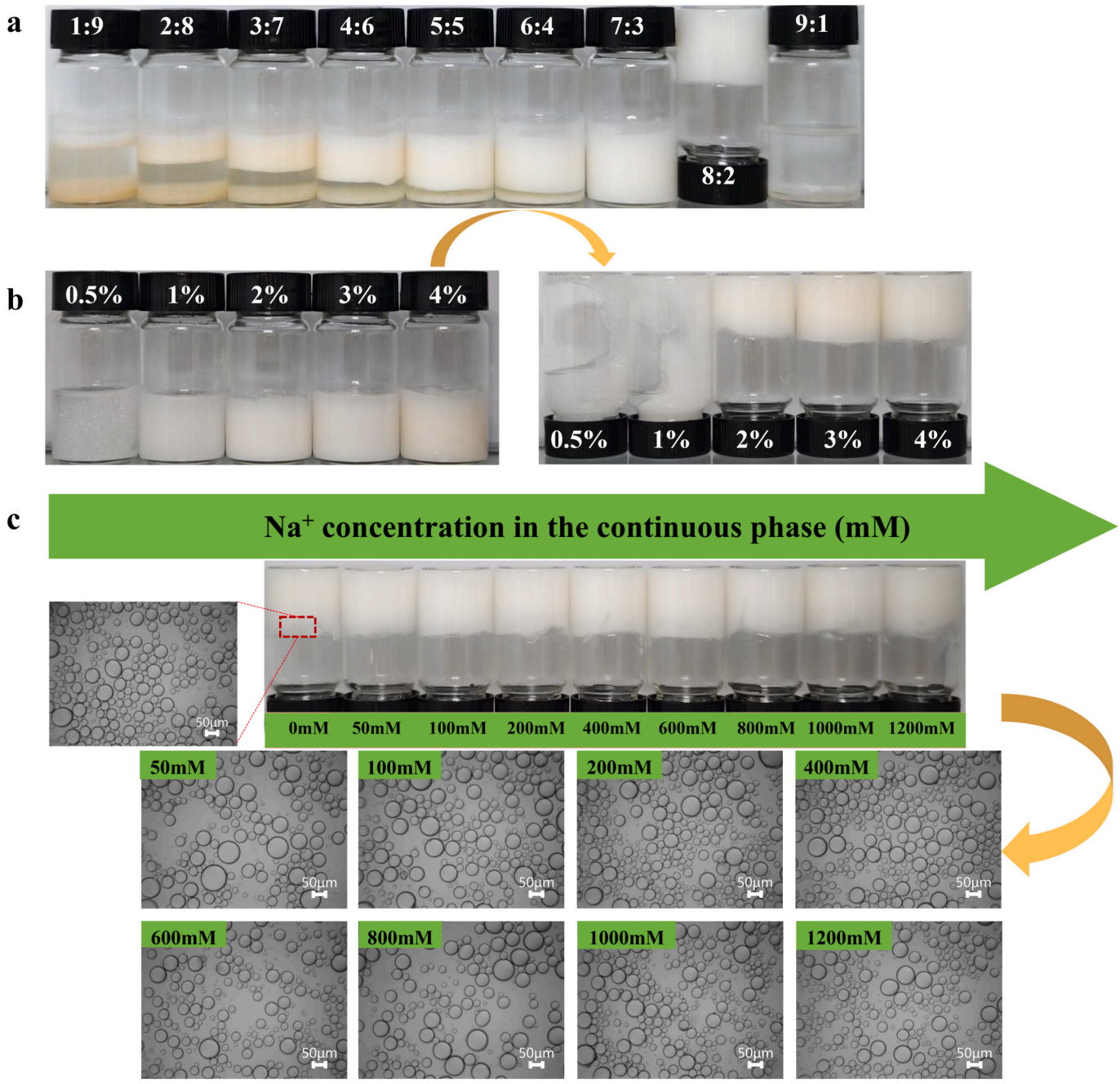

Fig. 7. The stability of MACNCs-stabilized Pickering emulsion after 6 months: (a) MACNCs-stabilized Pickering emulsion with aqueous phase concentration of 2wt% and φ range of 0.1-0.9; (b) MACNCs-HIPPEs with MACNCs concentration of 0.5-4wt% and φ value of 0.8 and (c) MACNCs-HIPPEs (MACNCs concentration of 2wt%, and φ of 0.8) to NaCl (0-1200 mM).

elastic module rather than the viscous module, which was the characteristic of the network materials [51]. The maximum G' and G" were found in the MACNCs-HIPPEs at φ of 0.8, also indicating the significance of higher φ.

3.3. *Influence of MACNCs dosages on the formation of MACNCs-HIPPEs*

In addition to the O/W ratios, the stabilizer dosages in the water phase (i.e., MACNCs concentrations) also influenced the stability of the as-prepared HIPPEs and were thus studied. Fig. 4 shows the digital photos, optical microscopy images, and the rheology of the collected MACNCs-HIPPEs. The emulsions can be formed at φ of 0.8 when the MACNCs concentrations range from 0.5% to 4%. Moreover, the emulsions transformed to the HIPPEs when the MACNCs concentrations were 2, 3, and 4% (Fig. 4a). With the increase in MACNCs concentration, the droplet size of MACNCs-HIPPEs decreased gradually (Fig. 4b and Fig. S6), which was caused by the rise in coverage of MACNCs particle at the oil-water interface [52]. This indicated that the increase in particle concentration was conducive to forming HIPPEs with greater rigidity and stability. Similar results can be found in the published data [40,53].

The rheological measurements were also performed for the MACNCs-HIPPEs with MACNCs concentrations of 2, 3, and 4%. All the G' were higher than G" in the low strain range (Fig. 4c), which manifested the elastic behavior and solid-like properties of the obtained Pickering emulsions [48]. Moreover, the G' of emulsion prepared at a MACNCs concentration of 1% was much smaller than that of MACNCs-HIPPEs

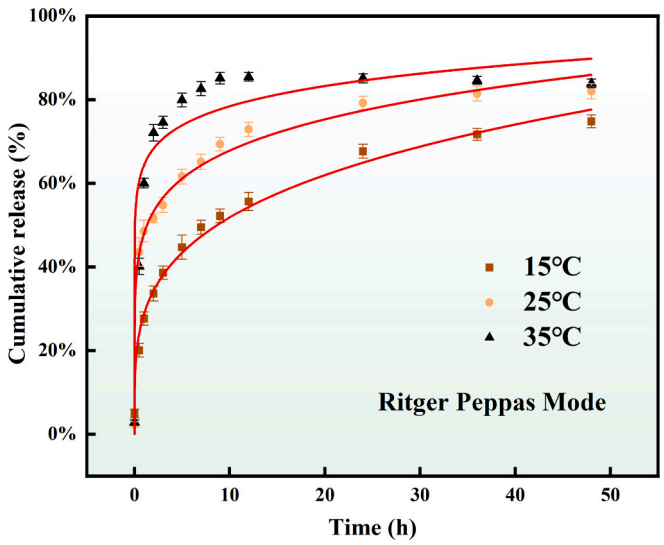

Fig. 8. Ritger-Peppas kinetics model that fitted experimental data of IMI@MACNCs-HIPPEs at different temperatures.

Table 1
Kinetics parameters of different models for IMI release from IMI@MACNCs-HIPPEs at different temperatures.

Kinetics models	The parameters	The release temperature		
		15°C	25°C	35°C
Zero-order model	K_1	0.0129	0.0173	0.0142
	R_1^2	0.7170	0.4827	0.4005
First-order model	K_2	0.6708	0.7394	0.8367
	R_2^2	0.9135	0.9678	0.9950
Higuchi model	K_3	0.1009	0.1362	0.1207
	R_3^2	0.9199	0.7864	0.6634
R-P model	n	0.2574	0.1508	0.0864
	R_4^2	0.9859	0.9955	0.9775

(Fig. 4c), indicating that the higher MACNCs concentration contributed to the formation of HIPPEs. The frequency dependence test of Pickering emulsions also showed that the G' were higher than G" (Fig. 5d). This result indicated that the elastic module played a dominant role and the network structures were formed in the Pickering emulsions [51]. The phenomenon was induced by the increasing coverage of the oil-water interface with the improvement of MACNCs concentration. The potential non-covalent interaction among MACNCs particles (e.g., electrostatic repulsion and hydrophobic force) led to the formation of a high internal phase emulsion network structure, which increased the viscosity of the emulsion, reduced the agglomeration of droplets and thus increased the modulus of the emulsion [54,55].

3.4. The stability of as-prepared MACNCs-HIPPEs to high-concentration salt

The surface-charged CNCs-stabilized Pickering emulsions generally showed salt responsiveness due to the widely exposed surface charge that can be shielded by salt ions [38]. This is an interesting performance but the opposite of the pesticide delivery due to the salt ions on the leaf surface. Below is the determination of salt responsiveness, and the results are shown in Fig. 5. The MACNCs-HIPPEs were prepared with 2% of MACNCs concentration at φ of 0.8, followed by adding NaCl to adjust the concentration to 0-1200 mM. All the emulsions were HIPPEs no matter what dosages of NaCl were added (Fig. 5a). It can be seen from the comparison of optical microscopy images that all the size of MACNCs-HIPPEs have almost no change and MACNCs-HIPPEs have no oil leakage or emulsion breaking (Fig. 5b and Fig. S7), may because MACNCs in the volume phase interacted with MACNCs in the droplet and the spatial repulsions among droplets were the main force maintaining MACNCs-HIPPEs rather than the electrostatic repulsion [41,56].

3.5. The micromorphology of MACNCs-HIPPEs

According to the above experiments, MACNCs-HIPPEs with the best stability (MACNCs concentration of 2wt%, φ of 0.8, and without NaCl) was selected for cryo-SEM to observe the microscopic distribution of the emulsion (Fig. 6). Most of the emulsion droplets significantly appeared as an independent sphere with a diameter of about 50 μm, which was surrounded by the freezing water. MACNCs can form a smooth and curved interface film with a network structure on the surface of the droplets and produce many adhesion points between the oil droplets. A network with linear branches is structured like a tentacle, connecting oil droplets together to stabilize the interface in the form of a mesh membrane with branches [57]. MACNCs, which are not tightly adsorbed on the oil-water interface, formed a dense three-dimensional network structure between droplets through electrostatic, hydrophobic, and hydrogen bonding, which hindered the aggregation of droplets [58]. Moreover, high rheological properties can limit the movement and agglomeration of the emulsion droplets, thus improving the stability of the emulsion. In addition, the storage modulus (G') is much higher than the loss modulus (G"), showing a typical gel-like behavior, which is also conducive to the stability of the high internal phase Pickering emulsion.

3.6. Storage stability

Storage stability is the basic judgment for a formulation in the applications, and here we determined the storage stability of the MACNCs-stabilized Pickering emulsions after storage for 6 months. Fig. 7a and b show the storage stability of the as-prepared Pickering emulsions at different O/W ratios or MACNCs dosages. Compared with the fresh emulsions (Fig. 3a and Fig. 4a), all the Pickering emulsions could be steadily stored for 6 months without visible changes. Also, the storage

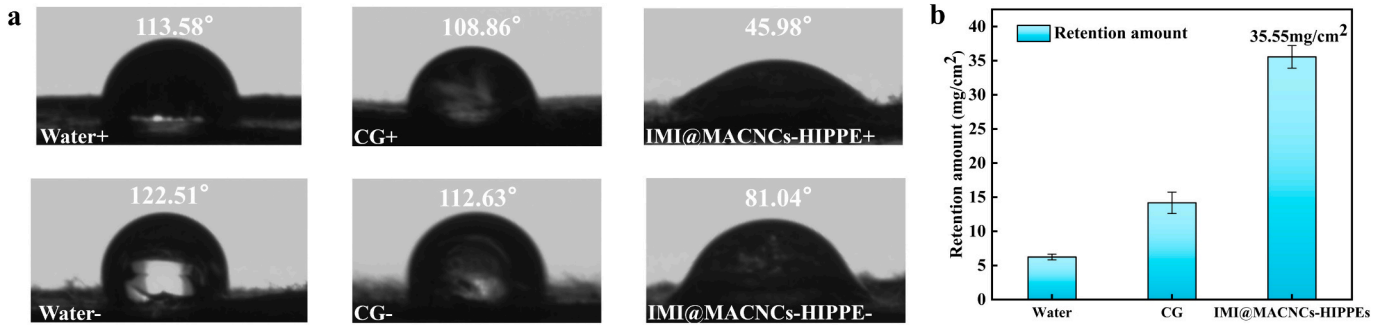

Fig. 9. Spread and retention of IMI@MACNCs-HIPPEs on the surface of cotton leaf: (a) contact angles (+ and - indicate the front and back sides of cotton leaves); (b) retention amount of IMI@MACNCs-HIPPEs.

stability of the NaCl-added Pickering emulsions was also determined, and the results are shown in Fig. 7c. The digital photos and optical microscopy images did not manifest macro or micro changes, including the grain diameter of the emulsion droplet.

3.7. Sustained-release performance of IMI@MACNCs-HIPPEs

IMI, a broad-spectrum insecticide, was in situ loaded into MACNCs-HIPPEs, and the slow-release performance of IMI was studied by in vitro experiments. The release process of IMI from IMI@MACNCs-HIPPEs can be divided into three parts: burst release stage, sluggish release stage, and equilibrium release stage (Fig. 8). Moreover, all the release systems presented clear burst releases in the methyl alcohol media at different release temperatures. To describe the release processes, the kinetics studies were performed, as shown in Fig. 8. The parameters of the kinetics models are listed in Table 1. The R_4^2 values of the R-P model were all higher than 0.97, indicating the feasibility of this model. Moreover, n, the diffusion exponent, were all much smaller than 0.43, which manifested the Fickian diffusion-controlled mechanism in the release processes.

The first-order kinetics model can also describe the release process well due to the acceptable R_2^2 values that were all greater than 0.91, also exhibiting the significance of differential concentration gradient. The R_2^2 values of the first-order kinetics model were clearly enlarged with the increase in release temperature, viz., the sustained release of IMI from the HIPPEs was also influenced by other factors except the differential concentration. Fig. 8 also revealed that cumulative release ratios were positively related to the temperature. These phenomena might be induced by the viscosity change of liquid paraffin at different temperatures, which significantly influence the diffusion of IMI [59].

Generally, higher temperatures contributed to pest propagation (e.g., aphids), and the requirements for insecticide dose consequently increased [60,61]. Thus, this thermo-responsiveness of the IMI@MACNCs-HIPPEs was suitable for crop applications. Overall, the IMI@MACNCs-HIPPEs could release IMI for more than 50 h, which is much better than the CNCs-stabilized Pickering emulsion-based release systems [38].

3.8. Spread and retention of IMI@MACNCs-HIPPEs on the leaf surface

The spread and retention of pesticide formulations significantly influenced the utilization rate of pesticides, which can be improved by adjusting the static contact angle. Fig. 9a shows the contact angles of water, IMI@MACNCs-HIPPEs, and commercial IMI suspension (CG) on the leaf surface. For water and CG, the contact angles were all greater than 90°, whether on the front or back of cotton leaves, indicating the incompatibility to the leaf surface. The IMI@MACNCs-HIPPEs presented a much smaller contact angle on the front of the leaf (45.98°). Thus, the IMI@MACNCs-HIPPEs had good spreading properties and were more easily attached to the leaves, which can effectively improve the utilization rate of IMI. Moreover, the contact angle of the back face was still close to 90° but much smaller than that of water and CG due to the villous structure.

The amount of leaf retention also indicated the residue of pesticides on crops. The cotton leaves were quickly removed by dipping into the IMI@MACNCs-HIPPEs, and droplets were only attached to the surface of the leaves. The retention amount of IMI@MACNCs-HIPPEs on cotton leaves was much greater than that of water and CG, reaching 35.55 mg/m^2 (Fig. 9b), which significantly reduced the use of pesticides and the consequent environmental issues. Moreover, we recorded videos of the water droplets and IMI@MACNCs-HIPPEs on a leaf surface with an angle of 60° to illustrate the specific retention (videos 1 and 2, supporting information). It is clear that the IMI@MACNCs-HIPPEs can stay on the leaf surface, but the water droplets just roll off the leaf surface. Thus, IMI@MACNCs-HIPPEs had high stability and modulus that was conducive to applying pesticide preparations because the considerable rheological energy can dissipate the system energy, thereby increasing the retention rate of pesticides in the leaves [62,63].

4. Conclusion

The cotton-derived CNCs were modified by MA to obtain the MACNCs that were used to form Pickering emulsions. The grafting content was calculated as 0.27 mmol/g, and the contact angle increased from 52.7° to 73.0°. The zeta potential of MACNCs only shifted from -33.91 mV to -29.3 mV without clear agglomeration even though the NaCl concentration was as high as 1000 mmol/L (i.e., 58.5 mg/mL). The HIPPEs were obtained when the φ was 0.8 and MACNCs concentration was 2wt%, which showed excellent salt stability (NaCl, 1200 mM) and significant storage stability (60 days). The typical three-dimensional structure of HIPPEs can also be seen by cryo-SEM. The IMI can continually be released from IMI@MACNCs-HIPPEs for more than 50 h at 15°C, 25°C, and 35°C; the release process was also significantly influenced by the release temperature. The contact angles of IMI@MACNCs-HIPPEs on the front and back of cotton leaf were 45.98° and 81.04° which were much smaller than that of water and CG. The retention amount of IMI@MACNCs-HIPPEs on cotton leaves was much greater than that of water and CG, reaching 35.55 mg/m^2. Thus, the present MACNCs-HIPPEs showed excellent potential in delivering IMI and can be promoted to other lipophilic pesticides.

CRediT authorship contribution statement

Chao Wu: Writing – original draft, Resources, Methodology, Investigation, Formal analysis, Data curation, Conceptualization. **Jun Li:** Writing – original draft, Visualization, Validation, Supervision, Resources, Methodology, Funding acquisition, Formal analysis. **Jia-wei Ding:** Methodology, Formal analysis, Data curation. **Hui Jiang:** Resources, Formal analysis, Data curation. **Hui-fen Su:** Investigation, Data curation. **De-qiang Li:** Visualization, Validation, Resources, Methodology, Investigation, Funding acquisition, Formal analysis, Data curation.

Declaration of competing interest

The authors declare no competing financial interests.

Data availability

Data will be made available on request.

Acknowledgment

The present work was supported by the Project of Tianshan Innovation Team Plan (No. 2023D14020); National Nature Science Foundation of China (No. 32160352); Natural Science Foundation of Xinjiang Uygur Autonomous Region, China (No. 2022D01A175).

Appendix A. Supplementary data

Supplementary data to this article can be found online at https://doi.org/10.1016/j.ijbiomac.2024.132971.

References

[1] C. Thiour-Mauprivez, F. Martin-Laurent, C. Calvayrac, L. Barthelmebs, Effects of herbicide on non-target microorganisms: towards a new class of biomarkers? Sci. Total Environ. 684 (2019) 314–325, https://doi.org/10.1016/j.scitotenv.2019.05.230.

[2] M. Zhao, L. Zhao, J.-P. Cao, W. Jiang, J.-X. Xie, C. Zhu, S.-Y. Wang, Y.-L. Wei, X.-Y. Zhao, H.-C. Bai, Water-involved tandem conversion of aryl ethers to alcohols over metal phosphide catalyst, Chem. Eng. J. 435 (2022) 134911, https://doi.org/10.1016/j.cej.2022.134911.

[3] M.A.M. Gruber, D. Santoro, M. Cooling, P.J. Lester, B.D. Hoffmann, C. Boser, L. Lach, A global review of socioeconomic and environmental impacts of ants

reveals new insights for risk assessment, Ecol. Appl. 32 (2022) e2577, https://doi.org/10.1002/eap.2577.
[4] R. Tao, C. You, Q. Qu, X. Zhang, Y. Deng, W. Ma, C. Huang, Recent advances in the design of controlled- and sustained-release micro/nanocarriers of pesticide, Environ. Sci.: Nano 10 (2023) 351–371, https://doi.org/10.1039/D2EN00446A.
[5] D.-X. Zhang, J. Du, R. Wang, J. Luo, T.-F. Jing, B.-X. Li, W. Mu, F. Liu, Y. Hou, Core/shell dual-responsive nanocarriers via iron-mineralized electrostatic self-assembly for precise pesticide delivery, Adv. Funct. Mater. 31 (2021) 2102027, https://doi.org/10.1002/adfm.202102027.
[6] A.E. Kaziem, Y. Gao, Y. Zhang, X. Qin, Y. Xiao, Y. Zhang, H. You, J. Li, S. He, α-Amylase triggered carriers based on cyclodextrin anchored hollow mesoporous silica for enhancing insecticidal activity of avermectin against Plutella xylostella, J. Hazard. Mater. 359 (2018) 213–221, https://doi.org/10.1016/j.jhazmat.2018.07.059.
[7] H.K. Frederiksen, H.G. Kristensen, M. Pedersen, Solid lipid microparticle formulations of the pyrethroid gamma-cyhalothrin—incompatibility of the lipid and the pyrethroid and biological properties of the formulations, J. Control. Release 86 (2003) 243–252, https://doi.org/10.1016/S0168-3659 (02)00406-6.
[8] D. Patel, S.S. Zode, A.K. Bansal, Formulation aspects of intravenous nanosuspensions, Int. J. Pharm. 586 (2020) 119555, https://doi.org/10.1016/j.ijpharm.2020.119555.
[9] Y. Zhang, C. Guo, L. Liu, J. Xu, H. Jiang, D. Li, J. Lan, J. Li, J. Yang, Q. Tu, X. Sun, M. Alamgir, X. Chen, G. Shen, J. Zhu, J. Tao, ZnO-based multifunctional nanocomposites to inhibit progression and metastasis of melanoma by eliciting antitumor immunity via immunogenic cell death, Theranostics 10 (2020) 11197–11214, https://doi.org/10.7150/thno.44920.
[10] D.-P. Wang, Z.-J. Wang, R. Zhao, C.-X. Lin, Q.-Y. Sun, C.-P. Yan, X. Zhou, J.-M. Cao, Silica nanomaterials induce organ injuries by Ca2+-ROS-initiated disruption of the endothelial barrier and triggering intravascular coagulation, Part. Fibre Toxicol. 17 (2020) 12, https://doi.org/10.1186/s12989-020-00340-8.
[11] G.-H. Chen, C.-C. Song, T. Zhao, C. Hogstrand, X.-L. Wei, W.-H. Lv, Y.-F. Song, Z. Luo, Mitochondria-dependent oxidative stress mediates ZnO nanoparticle (ZnO NP)-induced mitophagy and lipotoxicity in freshwater teleost fish, Environ. Sci. Technol. 56 (2022) 2407–2420, https://doi.org/10.1021/acs.est.1c07198.
[12] J. Zhang, W. Song, J. Guo, J. Zhang, Z. Sun, F. Ding, M. Gao, Toxic effect of different ZnO particles on mouse alveolar macrophages, J. Hazard. Mater. 219-220 (2012) 148–155, https://doi.org/10.1016/j.jhazmat.2012.03.069.
[13] R. Ma, Y. Qi, X. Zhao, X. Li, X. Sun, P. Niu, Y. Li, C. Guo, R. Chen, Z. Sun, Amorphous silica nanoparticles accelerated atherosclerotic lesion progression in ApoE−/− mice through endoplasmic reticulum stress-mediated CD36 up-regulation in macrophage, Part. Fibre Toxicol. 17 (2020) 50, https://doi.org/10.1186/s12989-020-00380-0.
[14] S. Tripathi, A. Bhattacharya, R. Singh, R.F. Tabor, Rheological behavior of high internal phase water-in-oil emulsions: effects of droplet size, phase mass fractions, salt concentration and aging, Chem. Eng. Sci. 174 (2017) 290–301, https://doi.org/10.1016/j.ces.2017.09.016.
[15] S.A. Kedzior, V.A. Gabriel, M.A. Dubé, E.D. Cranston, Nanocellulose in emulsions and heterogeneous water-based polymer systems: a review, Adv. Mater. 33 (2021) 2002404, https://doi.org/10.1002/adma.202002404.
[16] L. Ma, L. Zou, D.J. McClements, W. Liu, One-step preparation of high internal phase emulsions using natural edible Pickering stabilizers: gliadin nanoparticles/gum Arabic, Food Hydrocoll. 100 (2020) 105381, https://doi.org/10.1016/j.foodhyd.2019.105381.
[17] J. Shin, J.-W. Lee, S.-M. Seo, J. Hyun, I.-K. Park, Larvicidal activities of Cnidium officinale Makino extract encapsulated with cellulose nanocrystal-stabilized Pickering emulsion against Aedes albopictus Skuse, a vector of Zika virus, Ind. Crop. Prod. 204 (2023) 117263, https://doi.org/10.1016/j.indcrop.2023.117263.
[18] K. Chen, S. Yuan, D. Wang, Y. Liu, F. Chen, D. Qi, Basic amino acid-modified lignin-based biomass adjuvants: synthesis, emulsifying activity, ultraviolet protection, and controlled release of avermectin, Langmuir 37 (2021) 12179–12187, https://doi.org/10.1021/acs.langmuir.1c02113.
[19] F. Jiang, A.R. Esker, M. Roman, Acid-catalyzed and solvolytic desulfation of H2SO4-hydrolyzed cellulose nanocrystals, Langmuir 26 (2010) 17919–17925, https://doi.org/10.1021/la1028405.
[20] L. Zhou, H. He, M.-C. Li, S. Huang, C. Mei, Q. Wu, Enhancing mechanical properties of poly (lactic acid) through its in-situ crosslinking with maleic anhydride-modified cellulose nanocrystals from cottonseed hulls, Ind. Crop. Prod. 112 (2018) 449–459, https://doi.org/10.1016/j.indcrop. 2017.12.044.
[21] D. Da Silva Perez, S. Montanari, M.R. Vignon, TEMPO-mediated oxidation of cellulose III, Biomacromolecules 4 (2003) 1417–1425, https://doi.org/10.1021/bm034144s.
[22] G. Sèbe, F. Ham-Pichavant, G. Pecastaings, Dispersibility and emulsion-stabilizing effect of cellulose nanowhiskers esterified by vinyl acetate and vinyl Cinnamate, Biomacromolecules 14 (2013) 2937–2944, https://doi.org/10.1021/bm400854n.
[23] J. Dredán, I. Antal, I. Rácz, Evaluation of mathematical models describing drug release from lipophilic matrices, Int. J. Pharm. 145 (1996) 61–64, https://doi.org/10.1016/S0378-5173(96)04725-4.
[24] D. Xiao, W. Liang, Z. Xie, J. Cheng, Y. Du, J. Zhao, A temperature-responsive release cellulose-based microcapsule loaded with chlorpyrifos for sustainable pest control, J. Hazard. Mater. 403 (2021) 123654, https://doi.org/10.1016/j.jhazmat.2020.123654.
[25] W. Guan, W. Zhang, L. Tang, Y. Wang, H. Cui, Fabrication of novel avermectin nanoemulsion using a polyurethane emulsifier with cleavable disulfide bonds, J. Agric. Food Chem. 66 (2018) 6569–6577, https://doi.org/10.1021/acs.jafc.7b01427.
[26] Y. Jiang, Y. Zhu, F. Li, J. Du, Q. Huang, D. Sun-Waterhouse, D. Li, Antioxidative pectin from hawthorn wine pomace stabilizes and protects Pickering emulsions via forming zein-pectin gel-like shell structure, Int. J. Biol. Macromol. 151 (2020) 193–203, https://doi.org/10.1016/j.ijbiomac.2020.02.164.
[27] B. Pang, H. Liu, P. Liu, X. Peng, K. Zhang, Water-in-oil Pickering emulsions stabilized by stearoylated microcrystalline cellulose, J. Colloid Interface Sci. 513 (2018) 629–637, https://doi.org/10.1016/j.jcis.2017.11.079.
[28] J. Miao, Y. Yu, Z. Jiang, L. Zhang, One-pot preparation of hydrophobic cellulose nanocrystals in an ionic liquid, Cellulose 23 (2016) 1209–1219, https://doi.org/10.1007/s10570-016-0864-7.
[29] S.X. Peng, H. Chang, S. Kumar, R.J. Moon, J.P. Youngblood, A comparative guide to controlled hydrophobization of cellulose nanocrystals via surface esterification, Cellulose 23 (2016) 1825–1846, https://doi.org/10.1007/s10570-016-0912-3.
[30] W. Chen, H. Yu, Y. Liu, P. Chen, M. Zhang, Y. Hai, Individualization of cellulose nanofibers from wood using high-intensity ultrasonication combined with chemical pretreatments, Carbohydr. Polym. 83 (2011) 1804–1811, https://doi.org/10.1016/j.carbpol.2010.10.040.
[31] J.C.P. De Melo, E.C. Da Silva Filho, S.A.A. Santana, C. Airoldi, Maleic anhydride incorporated onto cellulose and thermodynamics of cation-exchange process at the solid/liquid interface, Colloids Surf. A Physicochem. Eng. Asp. 346 (2009) 138–145, https://doi.org/10.1016/j.colsurfa.2009.06.006.
[32] X. Xu, F. Liu, L. Jiang, J.Y. Zhu, D. Haagenson, D.P. Wiesenborn, Cellulose nanocrystals vs. cellulose nanofibrils: a comparative study on their microstructures and effects as polymer reinforcing agents, ACS Appl. Mater. Interfaces 5 (2013) 2999–3009, https://doi.org/10.1021/am302624t.
[33] Y. Zhou, Q. Jin, X. Hu, Q. Zhang, T. Ma, Heavy metal ions and organic dyes removal from water by cellulose modified with maleic anhydride, J. Mater. Sci. 47 (2012) 5019–5029, https://doi.org/10.1007/s10853-012-6378-2.
[34] C. Wu, J. Li, Y.-Q. Zhang, X. Li, S.-Y. Wang, D.-Q. Li, Cellulose dissolution, modification, and the derived hydrogel: a review, ChemSusChem 16 (2023) e202300518, https://doi.org/10.1002/cssc.202300518.
[35] Y. Zhang, D.-Q. Li, C.-X. Yang, Z.-W. Xiong, M. Tohti, Y.-Q. Zhang, H.-J. Chen, J. Li, Polymerization strategy for cellulose nanocrystals-based photonic crystal films with water resisting property, Int. J. Biol. Macromol. 265 (2024) 130793, https://doi.org/10.1016/j.ijbiomac.2024.130793.
[36] S. Spinella, A. Maiorana, Q. Qian, N.J. Dawson, V. Hepworth, S.A. McCallum, M. Ganesh, K.D. Singer, R.A. Gross, Concurrent cellulose hydrolysis and esterification to prepare a surface-modified cellulose nanocrystal decorated with carboxylic acid moieties, ACS Sustain. Chem. Eng. 4 (2016) 1538–1550, https://doi.org/10.1021/acssuschemeng.5b01489.
[37] P. Stenstad, M. Andresen, B.S. Tanem, P. Stenius, Chemical surface modifications of microfibrillated cellulose, Cellulose 15 (2008) 35–45, https://doi.org/10.1007/s10570-007-9143-y.
[38] C.-X. Yang, J. Li, Y.-Q. Zhang, C. Wu, D.-Q. Li, A pesticide sustained-release microcapsule from cellulose nanocrystal stabilized Pickering emulsion template, J. Appl. Polym. Sci. 140 (2023) e53716, https://doi.org/10.1002/app.53716.
[39] Q.-H. Chen, J. Zheng, Y.-T. Xu, S.-W. Yin, F. Liu, C.-H. Tang, Surface modification improves fabrication of Pickering high internal phase emulsions stabilized by cellulose nanocrystals, Food Hydrocoll. 75 (2018) 125–130, https://doi.org/10.1016/j.foodhyd.2017.09.005.
[40] T. Yang, J. Zheng, B.-S. Zheng, F. Liu, S. Wang, C.-H. Tang, High internal phase emulsions stabilized by starch nanocrystals, Food Hydrocoll. 82 (2018) 230–238, https://doi.org/10.1016/j.foodhyd.2018.04.006.
[41] H. Du Le, S.M. Loveday, H. Singh, A. Sarkar, Pickering emulsions stabilised by hydrophobically modified cellulose nanocrystals: responsiveness to pH and ionic strength, Food Hydrocoll. 99 (2020) 105344, https://doi.org/10.1016/j.foodhyd.2019.105344.
[42] L.Y. Lee, X.J. Lee, P.C. Chia, K.W. Tan, S. Gan, Utilisation of Cymbopogon citratus (lemon grass) as biosorbent for the sequestration of nickel ions from aqueous solution: equilibrium, kinetic, thermo- dynamics and mechanism studies, J. Taiwan Inst. Chem. Eng. 45 (2014) 1764–1772, https://doi.org/10.1016/j.jtice.2014.02.002.
[43] H. Zhao, J.H. Kwak, Y. Wang, J.A. Franz, J.M. White, J.E. Holladay, Effects of crystallinity on dilute acid hydrolysis of cellulose by cellulose ball-milling study, Energy Fuel 20 (2006) 807–811, https://doi.org/10.1021/ef050319a.
[44] J. Wu, X. Guan, C. Wang, T. Ngai, W. Lin, pH-responsive Pickering high internal phase emulsions stabilized by waterborne polyurethane, J. Colloid Interface Sci. 610 (2022) 994–1004, https://doi.org/10.1016/j.jcis.2021.11.156.
[45] V.O. Ikem, A. Menner, A. Bismarck, High internal phase emulsions stabilized solely by functionalized silica particles, Angew. Chem. Int. Ed. 48 (2009) 632, https://doi.org/10.1002/anie.200990003.
[46] H. Tan, L. Zhao, S. Tian, H. Wen, X. Gou, T. Ngai, Gelatin particle-stabilized high-internal phase emulsions for use in oral delivery systems: protection effect and in vitro digestion study, J. Agric. Food Chem. 65 (2017) 900–907, https://doi.org/10.1021/acs.jafc.6b04705.
[47] Y.-T. Xu, T.-X. Liu, C.-H. Tang, Novel Pickering high internal phase emulsion gels stabilized solely by soy β-conglycinin, Food Hydrocoll. 88 (2019) 21–30, https://doi.org/10.1016/j.foodhyd.2018.09.031.
[48] V. Vathsala, V. Saurabh, G. Kumar Choupdar, N. Upadhyay, S. Pal Singh, A. Dutta, C. Kaur, Black garlic particles as a natural pigment and emulsifier in a Pickering emulsion based low fat innovative mayonnaise: improved rheology and bioactivity, Food Res. Int. 173 (2023) 113484, https://doi.org/10.1016/j.foodres.2023.113484.
[49] P. Li, Y. Sui, X. Dai, Q. Fang, H. Sima, C. Zhang, Dynamic tannic acid hydrogel with self-healing and pH sensitivity for controlled release, Macromol. Biosci. 21 (2021) 2100055, https://doi.org/10.1002/mabi.202100055.

[50] H. Tan, G. Sun, W. Lin, C. Mu, T. Ngai, Gelatin particle-stabilized high internal phase emulsions as nutraceutical containers, ACS Appl. Mater. Interfaces 6 (2014) 13977–13984, https://doi.org/10.1021/am503341j.
[51] H. Dai, Y. Sun, X. Feng, L. Ma, H. Chen, Y. Fu, H. Wang, Y. Zhang, Myofibrillar protein microgels stabilized high internal phase Pickering emulsions with heat-promoted stability, Food Hydrocoll. 138 (2023) 108474, https://doi.org/10.1016/j.foodhyd.2023.108474.
[52] J. Wen, Y. Zhang, H. Jin, X. Sui, L. Jiang, Deciphering the structural network that confers stability to high internal phase Pickering emulsions by cross-linked soy protein microgels and their in vitro digestion profiles, J. Agric. Food Chem. 68 (2020) 9796–9803, https://doi.org/10.1021/acs.jafc.0c03586.
[53] F. Liu, J. Zheng, C.-H. Huang, C.-H. Tang, S.-Y. Ou, Pickering high internal phase emulsions stabilized by protein-covered cellulose nanocrystals, Food Hydrocoll. 82 (2018) 96–105, https://doi.org/10.1016/j.foodhyd.2018.03.047.
[54] M.N. Lee, H.K. Chan, A. Mohraz, Characteristics of Pickering emulsion gels formed by droplet bridging, Langmuir 28 (2012) 3085–3091, https://doi.org/10.1021/la203384f.
[55] J. Liu, J. Guo, H. Zhang, Y. Liao, S. Liu, D. Cheng, T. Zhang, H. Xiao, Z. Du, The fabrication, characterization, and application of chitosan–NaOH modified casein nanoparticles and their stabilized long-term stable high internal phase Pickering emulsions, Food Funct. 13 (2022) 1408–1420, https://doi.org/10.1039/D1FO02202D.
[56] X.-L. Li, W.-J. Liu, B.-C. Xu, B. Zhang, Simple method for fabrication of high internal phase emulsions solely using novel pea protein isolate nanoparticles: stability of ionic strength and temperature, Food Chem. 370 (2022) 130899, https://doi.org/10.1016/j.foodchem.2021.130899.
[57] J. Ding, Y. Li, Q. Wang, L. Chen, Y. Mao, J. Mei, C. Yang, Y. Sun, Pickering high internal phase emulsions with excellent UV protection property stabilized by Spirulina protein isolate nanoparticles, Food Hydrocoll. 137 (2023) 108369, https://doi.org/10.1016/j.foodhyd.2022.108369.
[58] T. Xu, Z. Gu, L. Cheng, C. Li, Z. Li, Y. Hong, Influence of degree of substitution of octenyl succinic anhydride starch on complexation with chitosan and complex-stabilized high internal phase Pickering emulsions, Food Hydrocoll. 139 (2023) 108526, https://doi.org/10.1016/j.foodhyd.2023.108526.
[59] A.D. Osborne, G. Porter, Diffusion studies in viscous media, Proc. R. Soc. Lond. A Math. Phys. Sci. 284 (1997) 9–16, https://doi.org/10.1098/rspa.1965.0048.
[60] A. Zamani, A. Talebi, Y. Fathipour, V. Baniameri, Temperature-dependent functional response of two aphid parasitoids, Aphidius colemani and Aphidius matricariae (Hymenoptera: Aphidiidae), on the cotton aphid, J. Pest. Sci. 79 (2006) 183–188, https://doi.org/10.1007/s10340-006-0132-y.
[61] S. Satar, U. Kersting, N. Uygun, Effect of temperature on development and fecundity of Aphis gossypii glover (Homoptera: Aphididae) on cucumber, J. Pest. Sci. 78 (2005) 133–137, https://doi.org/10.1007/s 10340-005-0082-9.
[62] J. De Ruiter, R. Lagraauw, D. van den Ende, F. Mugele, Wettability-independent bouncing on flat surfaces mediated by thin air films, Nat. Phys. 11 (2015) 48–53, https://doi.org/10.1038/nphys3145.
[63] J.C. Bird, R. Dhiman, H.-M. Kwon, K.K. Varanasi, Reducing the contact time of a bouncing drop, Nature 503 (2013) 385–388, https://doi.org/10.1038/nature12740.